Published in final edited form as:
Biomaterials. 2013 October ; 34(31): 7575–7583. doi:10.1016/j.biomaterials.2013.06.035.

Microstructural Constitutive Model of Active Coronary Media

Huan Chen[1], **Tong Luo**[1], **Xuefeng Zhao**[1], **Xiao Lu**[1], **Yunlong Huo**[2], and **Ghassan S. Kassab**[1,3,*]

[1]Department of Biomedical Engineering, Indiana University Purdue University Indianapolis, Indianapolis, IN 46202, United states

[2]Mechanics and Engineering Science, State Key Laboratory for Turbulence and Complex Systems, College of Engineering, Peking University, Beijing, 100871, China

[3]Department of Surgery, Cellular and Integrative Physiology, Indiana University Purdue University Indianapolis, Indianapolis, IN 46202, United states

Abstract

Although vascular smooth muscle cells (VSMCs) are pivotal in physiology and pathology, there is a lack of detailed morphological data on these cells. The objective of this study was to determine dimensions (width and length) and orientation of swine coronary VSMCs and to develop a microstructural constitutive model of active media. The dimensions, spatial aspect ratio and orientation angle of VSMCs measured at zero-stress state were found to follow continuous normal (or bimodal normal) distributions. The VSMCs aligned off circumferential direction of blood vessels with symmetrical polar angles 18.7°±10.9°, and the local VSMC deformation was affine with tissue-level deformation. A microstructure-based active constitutive model was developed to predict the biaxial vasoactivity of coronary media, based on experimental measurements of geometrical and deformation features of VSMCs. The results revealed that the axial active response of blood vessels is associated with multi-axial contraction as well as oblique VSMC arrangement. The present morphological data base is essential for developing accurate structural models and is seminal for understanding the biomechanics of muscular vessels.

Keywords

Biaxial vasoactivity; Vascular smooth muscle cell; Deformation; Morphology; Coronary artery

Introduction

The mechanical properties of an artery are determined by the vascular smooth muscle cells (VSMC) and the elastin and collagen fibers [1–3]. Elastin fibrils have relatively lower

*Correspondence: gkassab@iupui.edu.

stiffness and support blood vessels at low pressures while the collagen fibers are much stiffer to protect the artery from excessive dilation [4–6]. The VSMC provide negligible contributions to the passive properties of blood vessels [7–10], but are the predominate contributors of active behavior [9,11,12]. Although microstructure-based passive mechanical models of blood vessels have been studied extensively [13–17], the counterpart on active properties is not well developed. Mechanical studies of active vessels have been limited to phenomenological models [12,18–22], due to the complex micro-environment of VSMC and the coupled mechanical and chemical kinetics [23–25].

The majority of the active blood vessel constitutive models suggest uniaxial length-tension relationships in the circumferential direction as motivated by the circumferential arrangement of VSMC [4,26–28]. The orientation of VSMC, however, has been debated. While VSMC have been described as aligning in the circumferential direction in some studies [4,26–28], they were considered to be oblique in others [26,29–31]. Furthermore, some studies observed significant multi-axial responses of blood vessels during vasoconstriction [11,12,22,32,33]. A recent study showed that the porcine coronary artery displayed significant biaxial vasoconstriction induced by a K^+ physiological saline solution [12,22], where the active axial stress was more than half the circumferential stress. The significant axial active response, however, cannot be explained by the obliqueness of VSMC alignment alone. This implies that the biaxial vasoactivity may be induced by VSMC helical orientation as well as multi-axial active responses of individual VSMC [12,22,25].

In order to explain the overall mechanical behavior of coronary arteries (including the active media layer), the morphology of a vessel must be measured and used in a structure-based model. Here, we used confocal microscopy to visualize and quantify the morphology of VSMC at the zero-stress state (ZSS) as well as the deformation of individual VSMC under various pressure distensions. Based on measured geometrical features of VSMC, a microstructural constitutive model, including muscle contraction was proposed to describe the biaxial contraction of coronary arterial media.

Materials and Methods

Preparation of pressurized coronary artery

Six porcine hearts were obtained at a local slaughterhouse and transported to the laboratory in 4°C calcium-free physiological saline solution (PSS) immediately after the animals were sacrificed. The coronary arteries (2–3 mm in diameter) were dissected carefully form the hearts and the loose tissues were carefully removed. For each heart, six segments of ~2 cm in length were prepared for different distension pressures. A custom-made excess surface-area balloon tip catheter was inserted into each segment and distended to fully transmit pressure to the vessel lumen. The excess surface area of balloon ensured that no pressure was taken up by the balloon itself [6]. The distended segments were immersion-fixed in 0.8% methanol-free paraformaldehyde solution, the osmolarity of which was adjusted to 292±11 mOsm (verified by an automatic osmometer: Osmette A by Precision Systems, Inc.) with pH of 7.4. This fixative mimics the osmolarity of normal extracellular fluids (≈ 280 mOsm) to avoid cell shrinkage and swelling [34]. The segments were then fixed at room temperature for 48 hrs and later used for the preparation of histological sections.

Two 1 mm long rings were cut from each fresh segment before mechanical testing. One ring was fixed for 48 hrs, and the outer and inner diameters were measured before and after fixation to confirm that the fixative had negligible effect on the tissue. The other segment was cut off radially to reveal the ZSS [12,35] and the midwall circumference was measured. An additional ring was cut from the fixed distended segment to measure the loaded midwall circumference. Each sample was considered under one of six loading conditions: 1) ZSS; 2) no-load state (0 mmHg distension); 3) 40 mmHg distension; 4) 80 mmHg distension; 5) 120 mmHg distension; and 6) 160 mmHg distension.

Histology of media layer of coronary artery

Immediately after distention-fixation of the coronary arteries, 5×5 mm^2 cross-sections were sectioned from the segment and the circumferential direction was marked. The adventitia was peeled off carefully from the vessel to facilitate the staining and image processing since thin tissue is relatively easy to label and image. The main protein type of the cellular cytoskeleton, F-actin, and the cellular nucleus were labeled to track geometries of VSMC under various pressures. The sections were first incubated with 0.1% Triton X-100 solution for 5 min to permeabilize the cell membrane and rinsed 3 times with phosphate-buffered saline (PBS) (~300 mOsm, pH 7.4). The samples were then incubated with 1% bovine serum albumin (BSA) in PBS for 20 min to decrease nonspecific interactions prior to staining. They were then incubated with the staining buffer of Alexa Fluor 488 phalloidin (165 nM) and DAPI (150 nM) (Invitrogen, USA) in 1% BSA for 20 min, followed by extensive rinsing in PBS. The sections were wet mounted on microscope slides using a glycerin-water mixture. The slides were later viewed using a FV1000-MPE confocal microscope equipped with multiple laser options and a 60× 1.1NA water immersion objective (Olympus America, Center Valley, PA). Z-stack scans were implemented with a 1 μm step size between slices, and each slice covered an area of 211×211 μm^2 and was integrated over 4 frames to improve the signal-to-noise ratio. Each segment was scanned at 3 different locations for each loading condition.

Measurement of VSMC geometry

Geometries of VSMC—The orientation of the VSMC was measured using an automated algorithm. A center-line of the F-actin region was automatically extracted to measure the orientation angle of an individual cell (Fig. 1a), when anisotropic filtering was employed to improve the connectivity of the F-actin region [36]. This filtering smoothes along the object edges as opposed to other directions. Consequently, an F-actin region was filtered to a connected gray level region, and then thresholded to a binary region. The binary image of object center-lines is provided in Fig. 1b, where the bifurcations and disconnected segments were removed to form center-line of the cell. The MATLAB function ‘BWMORPH’ was used to compute orientation of the center-line with the circumferential direction taken as 0° and the axial direction as 90°. Finally, the histogram frequency distribution, based on binary pixels of the center-lines, is shown in Fig. 1c. Manual measurements of orientation angles were also used to validate the automatic measurement.

Manual measurements were made for dimensions of VSMC where the length and width were determined by the major and minor axes of each cell, respectively (Fig. 1a). The aspect

ratio, featuring the cell shape, was identified by the ratio of length to width of a given cell. Additionally, the orientation angle θ_{VSMC} of VSMC was defined as the angle between the direction of major axis and circumferential direction of cell.

Geometries of the nucleus: The RGB image (Blue) of the nucleus (Fig. 1d) was first converted to a binary image, where the nucleus-containing pixels were clearly distinguished from the background by median filtering (Fig. 1e). The MATLAB library function 'BWLABEL' was implemented to count and record connected components (the nuclei) and the function 'REGIONPROPS' was used to calculate the properties (e.g., orientation angle, length and width). The result was expressed as the mean, mean±SD (standard deviation), of all measured cells in the images. The significance of the difference between the parameter under various loads was evaluated by a one-way ANOVA test (SigmaStat 3.5), while the results were considered statistically different when $p < 0.05$.

Microstructure-based model of coronary media including VSMC contraction

The media segment was considered as a thin-walled elastic tube deformed in the circumferential and axial directions. Green strains are defined as $E_{\theta\theta}=(\lambda_\theta^2-1)/2$ and $E_{zz}=(\lambda_z^2-1)/2$, where $\lambda_\theta = \tau/\Gamma$ is the circumferential stretch ratio (τ refers to the midwall circumference of the loaded vessel and Γ refers to that at ZSS), and $\lambda_z = L/L_o$ is the axial stretch ratios with L and L_o being axial lengths in loaded and no-load states, respectively. A previously proposed structural constitutive model was used to describe the mechanical response of passive coronary media (17,37), which contains isotropic inter-lamellar (IL) elastin networks and helically oriented collagen fibers:

$$W_E(\mathbf{E})=\frac{f_E}{\pi}\int_{-\frac{\pi}{2}}^{\frac{\pi}{2}} w_E[e_E(\theta_E)]d\theta_E, \quad (1)$$

$$W_C(\mathbf{E})=\frac{f_C}{2}\{w_C[e_C(\theta_C)]+w_C[e_C(-\theta_C)]\}, \quad (2)$$

where w_E and w_C are the strain energy of elastin struts and collagen fibers, depending on uniaxial fiber strain e_s ($s = E,C$, denoting elastin and collagen, respectively). θ_s is the fiber orientation angle (corresponding unit vector denoted by $\vec{\mathbf{n}}^s$) and f_s is the volume fraction. The fiber strain was determined by $e_s = \vec{\mathbf{n}}^s \cdot \mathbf{E} \cdot \vec{\mathbf{n}}^s$ with assuming affine deformation (i.e., a fiber is assumed to rotate and stretch in the same way as the bulk tissue). The linear stress-strain relation of elastin was considered as $\partial w_E/\partial e_E = k_E e_E$ while the nonlinear relation of collagen was considered as $\partial w_C/\partial e_C = k_C e_C^{N_C}$, with the material parameter k_E representing the stiffness of the elastin, and k_C and N_C representing the stiffness and nonlinear parameter of collagen. The passive strain energy of the coronary media $W_{passive}$ was calculated by taking the sum of the strain energies of the elastin and collagen networks; i.e., $W_{passive}(\mathbf{E}) = W_E(\mathbf{E})+W_C(\mathbf{E})$, and the second Piola-Kirchhoff stress was accordingly determined by $\mathbf{S}_{passive} = \partial W_{passive}(\mathbf{E})/\partial \mathbf{E}$, and given by:

$$S_{\theta\theta passive}=\frac{k_E}{8}(3E_{\theta\theta}+E_{zz})+k_C cos^2\theta_C(cos^2\theta_C E_{\theta\theta}+sin^2\theta_C E_{zz})^{N_C}, \quad (3a)$$

$$S_{zz passive}=\frac{k_E}{8}(E_{\theta\theta}+3E_{zz})+k_C sin^2\theta_C(cos^2\theta_C E_{\theta\theta}+sin^2\theta_C E_{zz})^{N_C}. \quad (3b)$$

where $S_{\theta\theta passive}$ and $S_{zz passive}$ are passive circumferential and axial stresses, respectively.

The total strain energy of media is the sum of the active and passive contributions; i.e., $W_{total} = W_{passive}+W_{active}$. The function W_{active} is the active strain energy of vessels and is dominantly contributed by active VSMC. Taking into consideration helical arrangement of VSMC, the active strain energy can be given as:

$$W_{active}=\frac{f_{VSMC}}{2}\left\{\int_0^{\frac{\pi}{2}}\Re(\theta_{VSMC})w_{VSMC}(\theta_{VSMC})d\theta_{VSMC}+\int_{-\frac{\pi}{2}}^{0}\Re(-\theta_{VSMC})w_{VSMC})d\theta_{VSMC}\right\}, \quad (4)$$

where Θ_{VSMC} is the orientation angle of VSMC, $\Re(\Theta_{VSMC})$ is the two-dimensional orientation distribution of VSMC, w_{VSMC} is multi-axial strain energy of a single VSMC and f_{VSMC} is the volume fraction. A two-dimensional generalization of the uniaxial length-tension relation of active VSMC [20] was used to account for the multi-axial active response of VSMC [12,22]. Two families of helical VSMC with symmetrical polar angles, $\pm\Theta_{VSMC}$, were considered for simplicity (i.e., span of orientational distribution of VSMC is zero). Thus, the active strain energy of VSMC can be written as follows:

$$W_{active}(\lambda_{VSMC},\lambda^{\perp}_{VSMC})=\frac{f_{VSMC}}{2}\left\{w_{VSMC}\left\{\lambda_{VSMC},\lambda^{\perp}_{VSMC}\right\}(\theta_{VSMC})+w_{VSMC}\left\{\lambda_{VSMC},\lambda^{\perp}_{VSMC}\right\}(-\theta_{VSMC})\right\}, \quad (5)$$

$$\text{With} w_{VSMC}(\theta_{VSMC})=AC_{act}\left\{\text{Erf}\left(\frac{\lambda_{VSMC}(\theta_{VSMC})-b_3}{b_1}+\frac{\lambda^{\perp}_{VSMC}(\theta_{VSMc})-b_4}{b_2}\right)+1\right\}, \quad (6)$$

where $\lambda_{VSMC}=\sqrt{\vec{\mathbf{n}}^{VSMC}\cdot(\mathbf{F}^T\cdot\mathbf{F})\cdot\vec{\mathbf{n}}^{VSMC}}$ is the longitudinal stretch ratio of a VSMC (i.e., cell stretch), and $\lambda^{\perp}_{SMC}=\sqrt{\vec{\mathbf{n}}^{VSMC'}\cdot(\mathbf{F}^T\cdot\mathbf{F})\cdot\vec{\mathbf{n}}^{VSMC'}}$ is the transversal stretch ratio ($\mathbf{F}$ is deformation gradient). $\vec{\mathbf{n}}^{VSMC}$ and $\vec{\mathbf{n}}^{VSMC'}$ are the longitudinal and transversal vectors, respectively. A is the level of activation (0 is passive state and 1 is fully active), C_{act}, b_1, b_2, b_3 and b_4 are material constants, and Erf() is the Gauss error function. Accordingly, the active stress of coronary media is determined as the derivatives of the strain energy function; i.e., $\mathbf{S}_{active} = \partial W_{active}(\mathbf{E})/\partial\mathbf{E}$ and given by:

$$S_{\theta\theta active}=\frac{2AC_{act}}{\sqrt{\pi}}\left(\frac{cos^2\theta_{VSMC}}{b_1\lambda_{VSMC}}+\frac{sin^2\theta_{VSMC}}{b_2\lambda^{\perp}_{VSMC}}\right)\text{Exp}[-Q], \quad (7a)$$

$$S_{zzactive}=\frac{2AC_{act}}{\sqrt{\pi}}\left(\frac{sin^2\theta_{VSMC}}{b_1\lambda_{VSMC}}+\frac{cos^2\theta_{VSMC}}{b_2\lambda^{\perp}_{VSMC}}\right)\mathrm{Exp}[-Q]. \quad (7b)$$

where $S_{\theta\theta active}$ and $S_{zzactive}$ are the active circumferential and axial stresses of VSMC contraction, and $\mathrm{Q}=\left(\frac{\lambda_{VSMC}-b_3}{b_1}+\frac{\lambda^{\perp}_{VSMC}-b_4}{b_2}\right)^2$. Therefore, the total stress is the sum of passive (Eq. 3) and active stresses (Eq. 7): $\mathbf{S}_{total} = \mathbf{S}_{passive}+\mathbf{S}_{active}$.

We used biaxial data of coronary media obtained in our previous study (A = 1) [22] to determine the nine material parameters (the volume fraction f_E, f_C, f_{VSMC} are incorporated into the estimations of k_E, k_C, C_{act}, respectively). The media was considered as a thin cylindrical shell and the 2nd Piola-Kirchhoff circumferential stress obtained by experimental measurement was determined by $S^{exp}_{\theta\theta}=\frac{Pr_i}{h\lambda^2_\theta}$, where P is distension pressure, $r_i=\sqrt{r_o^2-\frac{A_o}{\pi\lambda_z}}$ is the inner radius in the loaded state, r_o is the outer radius in the loaded state, A_o is the wall area in a no-load state, and $h = r_o-r_i$ is the wall thickness in the loaded state. The axial stress was computed by $S^{exp}_{zz}=\frac{1}{\lambda^2_z}\left(\frac{Pr_i^2}{h(r_o+r_i)}+\frac{F}{\pi(r_o^2-r_i^2)}\right)$ with F presenting the axial force. The material parameters were determined by minimizing the square of the difference between the theoretical and experimental passive circumferential and axial 2nd Piola-Kirchhoff stresses. The four passive parameters $\{k_E, k_C, N_C, \theta_C\}$ were calculated firstly by:

$$Error_1=\sum_{n=1}^{N}\left[\left(S^{exp}_{\theta\theta passive}-S_{\theta\theta passive}\right)^2+\left(S^{exp}_{zzpassive}-S_{zzpassive}\right)^2\right] \quad (8)$$

where $S^{exp}_{\theta\theta passive}$ and $S^{exp}_{zzpassive}$ are the experimentally measured circumferential and axial stresses of the passive coronary media. The five active parameters $\{C_{act}, b_1, b_2, b_3, b_4\}$ were then identified by:

$$Error_2=\sum_{n=1}^{N}\left[\left(S^{exp}_{\theta\theta total}-S^{exp}_{\theta\theta passive}-S_{\theta\theta active}\right)^2+\left(S^{exp}_{zztotal}-S^{exp}_{zzpassive}-S_{zzactive}\right)^2\right] \quad (9)$$

where $S^{exp}_{\theta\theta total}$ and $S^{exp}_{zztotal}$ are the total circumferential and axial stresses of K^+ induced VSMC contraction. A limited-memory quasi-Newton method for large-scale optimization (L-BFGS method) [12,22] was employed to solve the above minimizations (Eqs. 8 and 9). The material parameters were determined for the five hearts individually, and the means of the five samples were presented as well.

Results

The difference between automatic and manual measurements of orientation angle was 4.1% and 3.3% for the no-load state and 80 mmHg distension, with no statistically significant difference between these two groups (P=0.54 and P=0.83) as shown in Fig. 1f. Moreover, no significant differences (P>0.05) were found between the outer diameter and thickness of specimen rings before and after fixation (outer diameter: 2.6±0.3 vs. 2.5±0.4; thickness:

0.5±0.09 vs. 0.5±0.1), suggesting that 0.8% methanol-free paraformaldehyde solution preserves the morphology of VSMC without shrinkage or swelling. The distributions of the geometrical parameters were analyzed based on 6 samples (18 scanning locations). Specifically, more than 30 individual cells were measured in each image such that over 500 cells were captured at each loading condition.

There was no significant structural heterogeneity between IL layers of coronary media. VSMC and the nuclei were both fusiform-shaped as shown in Figs. 1a and 3, and VSMC were more spindled with significantly larger tails. At ZSS, the histograms of geometrical parameters of VSMC and nuclei were plotted in Fig. 2, and their probability distribution functions were fitted to continuous normal distributions (Table 1). The length of individual VSMC was 56.0±10.3 μ*m* which is larger than that of the nuclei (15.0±4.7 μ*m*) while their widths were similar (3.9±0.7 μ*m* vs. 3.4±0.8 μ*m*) (Fig. 2a,b). The means of aspect ratio of the VSMC and the nuclei were 14.7±3.5 and 4.6±1.7, respectively, as plotted in Fig. 2c. VSMC aligned off the circumferential direction of the vessel with a bimodal distribution with a mean angle of ±18.7 ±10.9° (Fig. 2d), consistent with the angle of the nucleus, ±19.9±10.7°.

The VSMC of passive coronary media deformed significantly with an increase in distention pressure (Fig. 3). The cells gradually shifted in the circumferential direction at elevated pressure; i.e., reorienting to the loading direction. The VSMC were significantly stretched in the axial direction and became more spindled with longer tails (Fig. 3d,e) than those in the no-load state (Fig. 3a), while the nuclei did not significantly deform. Changes of geometries of VSMC and nuclei were quantified and plotted in Fig. 4, and the corresponding non-linear dependency on distension pressure was tabulated (Table 2). The length of VSMC increased significantly until distension pressure reached 80 mmHg ($P<0.05$ when distension pressure increased from 0 mmHg to 80mmHg, $P>0.05$ when pressure>80 mmHg), while the length of the nuclei increased relatively slightly ($P<0.05$ bellow 80mmHg pressure and $P>0.05$ after that), as shown in Fig. 4a. The widths of VSMC and the nuclei did not change significantly under all pressures ($P>0.05$). Accordingly, the aspect ratio of VSMC increased significantly at lower pressures ($P<0.05$) and plateaued at higher pressures ($P>0.05$), while that of the nuclei did not change significantly ($P>0.05$) as shown in Fig. 4b. The orientation angles of VSMC and the nuclei decreased significantly from the no-load state to 40 mmHg distension ($P<0.05$), while smaller changes were observed in a pressure range of 40–160 mmHg ($P>0.05$) (Fig. 4a). The mean orientation angle of VSMC became 13.0±2.6° at 80 mmHg and 11.9±3.0° at 160 mmHg pressure. There was no significant difference between the orientation of VSMC and the nuclei at each load ($P>0.05$).

The predicted reorientation of VSMC, determined by $\theta'_{VSMC}=arccos\left(\frac{cos\theta_{VSMC}\lambda_\theta}{\sqrt{cos^2\theta_{VSMC}\lambda_\theta^2+sin^2\theta_{VSMC}\lambda_z^2}}\right)$ (λ_z = 1.0 in experimental study), was also plotted in Fig. 4c, according to the affine deformation assumption. Correspondingly, the VSMC stretch ratio, determined by the ratio of cell length in the loaded state relative to ZSS, was predicted as $\lambda_{VSMC}=\sqrt{cos^2\theta_{VSMC}\lambda_\theta^2+sin^2\theta_{VSMC}\lambda_z^2}$. The relation between cell stretch

ratio and macroscopic tissue stretch ratio was given in Fig. 4d. The results (Figs. 4c and d) showed that model predictions of VSMC deformation agreed with experimental measurements ($P>0.05$).

The total, passive and active circumferential stresses of media were plotted in Figs. 5a and c for axial stretch ratio $\lambda_z = 1.2$ and $\lambda_z = 1.3$ respectively, while the corresponding axial stresses are shown in Figs. 5b and d. The experimental data averaged over 5 samples were presented by symbols (diamond, circle and solid triangle), and model predictions were presented by solid lines. Material parameters of individual collagen fibers, elastin network, and VSMC were listed in Tables 3 and 4. The predicted mean ratio of axial to circumferential active stresses of the media was 0.63±0.02 for $\lambda_z = 1.2$ and 0.59±0.02 for $\lambda_z = 1.3$ as compared to experimental measurement were 0.64±0.09 and 0.58±0.04, respectively. The mean ratio of a single VSMC (i.e.,b_1/b_2), however, was 0.4±0.06, smaller than that of the media. It was also found that the peak active circumferential stress of media (referred to optimal stretch ratio $\lambda_\theta^{'}$) slightly preceded the axial stress, while the peak active circumferential and axial stresses of individual VSMC occurred at the same stretch level. As shown in Fig. 5, the larger axial stretch ratio $\lambda_z = 1.3$ advanced VSMC contraction, with the maximal active circumferential and axial stress occurring at $\lambda_\theta^{'}=1.34$ and $\lambda_\theta^{'}=1.36$, respectively, earlier than that of $\lambda_\theta^{'}=1.39$ and $\lambda_\theta^{'}=1.41$ at $\lambda_z = 1.2$.

Discussion

The length and width of VSMC followed a normal distribution in coronary media, while the orientation angle showed a bimodal normal distribution, in line with previous observations of VSMC helical arrangement in vessels [29–31]. The VSMC orientation and distribution implies that VSMC constriction generates not only circumferential active stress, but also axial active responses in coronary arteries. The active axial stress has been previously ignored in most mechanical models of active blood vessels [19,20,38]. The morphological database was used to construct a microstructure-based model of active coronary media. This model accounts for passive material properties of individual collagen and elastin fibers, and passive and active VSMC.

The morphological-pressure relations of VSMC and nuclei were obtained for the length and orientation angle. The change of VSMC length increased sharply from the no-load state to 80 mmHg distention and became plateaued at higher pressure, consistent with that of the outer diameter of vessels. This suggests that recruited collagen fibers either in media or adventitia prevent the intact vessel as well as VSMC from overstretch at high pressure [4,6,39,40]. The reorientation of VSMC displayed similar non-linear dependency on distention pressure (Fig. 4c), gradually orienting towards the circumferential direction of the vessels with an increase in pressure. The orientation angle of the VSMC was about 13.0±2.6° at 80 mmHg pressure, suggesting that VSMC align slightly off the circumferential direction of vessels at physiological pressure. It should be noted that the physiological axial stretch ratio (about 1.3 for coronary arteries) leads to a large oblique arrangement of the VSMC from the vessel circumferential direction.

The deformation of individual VSMC was found to be affine (Figs. 4c and d). In blood vessels, VSMC connect with the extracellular matrix (ECM) via focal adhesion and the deformation thus strongly depends on ECM deformation as well as the macroscopic deformation of blood vessels. It is likely that flexible actin filaments deform with ECM through dense bodies in passive tissue such that collagen and elastin fibers follow affine deformation [41,42]. A pervious study showed that VSMC depend non-linearly on fiber deformation, based on changes in the aspect ratios of the nuclei under various biaxial loading conditions [42]. This conclusion, however, may be questionable since deformation of the nucleus is different from that of the cellular cytoskeleton, as shown in Fig. 4a. The deformation of the nuclei was not affine with tissue level deformation.

VSMC become stiffer during vasoconstriction due to the forces generated by actin-myosin interaction and tensile properties of cytoskeletal filaments increase significantly in contraction. Hence, the affine deformation assumption needs to be directly tested in active VSMC. Moreover, the elongation of the nuclei suggested that the tension developed by the cytoskeleton is transferred to the nuclei which may influence gene transcription and cellular phenotypes [28,43]. Consequently, the determination of strain and stress on individual VSMC is essential for better understanding of VSMC functions in normal and diseased arteries. This requires the development of microstructure based models to accurately predict the micro-environment of cells and nuclei.

The biaxial vasoactiviy of blood vessels determined in coronary arteries by Huo et al. [12,22] was also found in other experimental studies [11,32,33]. Lu and Kassab [11] found that there were significant axial force changes during vasomotions of carotid and femoral arteries by using an isovolumic myograph. A more recent study showed that VSMC vasoconstriction reduced artery buckling as compared with relaxed conditions [33], indicating that vasoactivity may shorten the artery in the axial direction (i.e., vessel become much stiffer in both circumferential and axial directions). These studies suggest that the biaxial vasoactivity of arteries is related to the helical structure of VSMC in muscular arteries. The ratio of active axial to circumferential stresses was predicted as $\frac{sin^2\theta_{VSMC}}{cos^2\theta_{VSMC}}=0.12$ for any axial stretch ratio λ_z, assuming a simple one-dimension constitutive law for active VSMC ($b_2 \rightarrow 0$ in Eq. (7)). This value, however, was significantly lower than experimental measurements. It suggests that there exists multi-axial VSMC vasoconstriction in coronary media, and that the biaxial vasoactivity is induced by oblique VSMC arrangement as well as multi-axial muscle vasoconstriction.

The axial active response was principally induced by the multi-axial contraction of VSMC, denoted by the mean ratio of transversal to axial active stress of a single muscle fiber $(\frac{b_1}{b_2}=0.4\pm0.06)$, while the oblique VSMC arrangement (θ_{VSMC} = 18.7°) contributed about 30%. With the influence of helical orientation of VSMC, the larger axial stretch ratio λ_z = 1.3 further stretches the oblique VSMC and the peak active stresses, thus occurs earlier than that of λ_z = 1.2 (Table 4). The present microstructural model, based on a structural passive model and a two-dimensional model of active VSMC [12,22], can accurately predict the biaxial vasoactivity of coronary media based on the measured microstructure.

Some limitations warrant discussion. First, the two-dimensional constitutive relation of individual active VSMC was based on a phenomenological constitutive model proposed by Huo et al. [12,22] to fit the biaxial responses of the K^+ induced vasoconstriction. In future studies, a three-dimensional structural constitutive model should be developed for active VSMC, where the material parameters have physical significance. The actin-myosin interaction is recognized as the fundamental mechanism of tension development in contractile cells and involves several signal transduction pathways. The constitutive law of VSMC is thus a combination of molecular biology and non-linear mechanics [23–25]. Second, the present model does not account for the VSMC in the lamella adjacent to intima or adventitia, where VSMC aligned towards the axial direction [28,44] and may contribute partially to the biaxial active response of blood vessels. In addition, a microstructure-based model of the entire vessel, should be integrated to investigate macro- and microscopic mechanical behaviors of active vessels [22,45]. Finally, experimental measurement of circumferential stretch ratio of coronary arteries was statistical since the midwall circumference at loaded states and ZSS were measured in different, albeit adjacent segments.

Conclusion

In summary, we present a systematic data base on the dimensions and orientation of VSMC of coronary media. The data was coupled with an active two-dimensional model to predict both circumferential and axial deformation. The proposed structural model accurately predicted the multi-axial mechanical responses of coronary media, and provides a more accurate framework for the biomechanics of blood vessels.

REFERENCES

1. Azuma T, Hasegawa M. A rheological approach to the architecture of arterial walls. Jpn J Physiol. 1971; 21:27–47. [PubMed: 5317235]
2. Azuma T, Oka S. Mechanical equilibrium of blood vessel walls. Am J Physiol. 1971; 221:1310–1318. [PubMed: 5124273]
3. Oka S, Azuma T. Physical theory of tension in thick-walled blood vessels in equilibrium. Biorheology. 1970; 7:109–117. [PubMed: 5484331]
4. Clark JM, Glagov S. Transmural organization of the arterial media. The lamellar unit revisited. Arteriosclerosis. 1985; 5:19–34. [PubMed: 3966906]
5. Glagov S, Vito R, Giddens DP, Zarins CK. Micro-architecture and composition of artery walls: relationship to location, diameter and the distribution of mechanical stress. J Hypertens Suppl. 1992; 10:101–104.
6. Zoumi A, Lu X, Kassab GS, Tromberg BJ. Imaging coronary artery microstructure using second-harmonic and two-photon fluorescence microscopy. Biophys J. 2004; 87:2778–2786. [PubMed: 15454469]
7. Roach MR, Burton AC. The reason for the shape of the distensibility curves of arteries. Can J Biochem Physiol. 1957; 35:681–690. [PubMed: 13460788]
8. Wolinsky H, Glagov S. Structural basis for the static mechanical properties of the aortic media. Circulation Research. 1964; 14:400–413. [PubMed: 14156860]
9. Matsumoto T, Nagayama K. Tensile properties of vascular smooth muscle cells: bridging vascular and cellular biomechanics. J Biomech. 2012; 45:745–755. [PubMed: 22177671]

10. Kochová P, Kuncová J, Svíglerová J, Cimrman R, Miklíková M, Liška V, et al. The contribution of vascular smooth muscle, elastin and collagen on the passive mechanics of porcine carotid arteries. Physiol Meas. 2012; 33:1335–1351. [PubMed: 22813960]
11. Lu X, Kassab GS. Vasoactivity of blood vessels using a novel isovolumic myograph. Ann Biomed Eng. 2007; 35:356–366. [PubMed: 17221307]
12. Huo Y, Cheng Y, Zhao X, Lu X, Kassab GS. Biaxial vasoactivity of porcine coronary artery. Am J Physiol Heart Circ Physiol. 2012; 302:H2058–H2063. [PubMed: 22427520]
13. Lanir Y. Constitutive equations for fibrous connective tissues. J Biomech. 1983; 16:1–12. [PubMed: 6833305]
14. Wuyts FL, Vanhuyse VJ, Langewouters GJ, Decraemer WF, Raman ER, Buyle S. Elastic properties of human aortas in relation to age and atherosclerosis: a structural model. Phys Med Biol. 1995; 40:1577–1597. [PubMed: 8532741]
15. Dahl SLM, Vaughn ME, Hu JJ, Driessen NJB, Baaijens FPT, Humphrey JD, et al. A microstructurally motivated model of the mechanical behavior of tissue engineered blood vessels. Ann Biomed Eng. 2008; 36:1782–1792. [PubMed: 18720007]
16. Lokshin O, Lanir Y. Micro and macro rheology of planar tissues. Biomaterials. 2009; 30:3118–3127. [PubMed: 19324407]
17. Hollander Y, Durban D, Lu X, Kassab GS, Lanir Y. Experimentally validated microstructural 3D constitutive model of coronary arterial media. J Biomech Eng. 2011; 133:031007. [PubMed: 21303183]
18. Rachev A, Hayashi K. Theoretical study of the effects of vascular smooth muscle contraction on strain and stress distributions in arteries. Ann Biomed Eng. 1999; 27:459–468. [PubMed: 10468230]
19. Zulliger MA, Rachev A, Stergiopulos N. A constitutive formulation of arterial mechanics including vascular smooth muscle tone. Am J Physiol Heart Circ Physiol. 2004; 287:1335–1343.
20. Carlson BE, Secomb TW. A theoretical model for the myogenic response based on the length-tension characteristics of vascular smooth muscle. Microcirculation. 2005; 12:327–338. [PubMed: 16020079]
21. Schmitz A, Böl M. On a phenomenological model for active smooth muscle contraction. J Biomech. 2011; 44:2090–2095. [PubMed: 21632055]
22. Huo Y, Zhao X, Cheng Y, Lu X, Kassab GS. Two-layer model of coronary artery vasoactivity. J Appl Physiol. 2013; 114:1451–1459. [PubMed: 23471951]
23. Gestrelius S, Borgström P. A dynamic model of smooth muscle contraction. Biophys J. 1986; 50:157–169. [PubMed: 3730500]
24. Yang J, Clark JW Jr, Bryan RM, Robertson C. The myogenic response in isolated rat cerebrovascular arteries: smooth muscle cell model. Med Eng Phys. 2003; 25:691–709. [PubMed: 12900184]
25. Stålhand J, Klarbring A, Holzapfel GA. A mechanochemical 3D continuum model for smooth muscle contraction under finite strains. J Theor Biol. 2011; 268:120–130. [PubMed: 20946904]
26. Wolinsky H, Glagov S. A lamellar unit of aortic medial structure and function in mammals. Circ Res. 1967; 20:99–111. [PubMed: 4959753]
27. Hansen TR, Dineen DX, Pullen GL. Orientation of arterial smooth muscle and strength of contraction of aortic strips from DOCA-hypertensive rats. Blood Vessels. 1980; 17:302–311. [PubMed: 7437523]
28. O'Connell MK, Murthy S, Phan S, Xu C, Buchanan J, Spilker R, et al. The threedimensional micro- and nanostructure of the aortic medial lamellar unit measured using 3D confocal and electron microscopy imaging. Matrix Biol. 2008; 27:171–181. [PubMed: 18248974]
29. Osborne-Pellegrin MJ. Some ultrastructural characteristics of the renal artery and abdominal aorta in the rat. J Anat. 1978; 125:641–652. [PubMed: 640965]
30. Rhodin, JAG. Architecture of the vessel wall. In: Bohr, DF.; Somlyo, AP.; Sparks, AV., editors. Handbook of physiology, section 2: The cardiovascular system, volume II. Bethesda: American physiology society; 1980. p. 1-31.
31. Fujiwara T, Uehara Y. The cytoarchitecture of the medial layer in rat thoracic aorta: a scanning electron-microscopic study. Cell Tissue Res. 1992; 270:165–172. [PubMed: 1423519]

32. Gaballa MA, Jacob CT, Raya TE, Liu J, Simon B, Goldman S. Large artery remodeling during aging: biaxial passive and active stiffness. Hypertension. 1998; 32(3):437–443. [PubMed: 9740608]
33. Hayman DM, Zhang J, Liu Q, Xiao Y, Han H-C. Smooth muscle cell contraction increases the critical buckling pressure of arteries. J Biomech. 2013; 46:841–844. [PubMed: 23261241]
34. Loqman MY, Bush PG, Farquharson C, Hall AC. A cell shrinkage artefact in growth plate chondrocytes with common fixative solutions: importance of fixative osmolarity for maintaining morphology. Eur Cell Mater. 2010; 19:214–227. [PubMed: 20473830]
35. Lu X, Pandit A, Kassab GS. Biaxial incremental homeostatic elastic moduli of coronary artery: two-layer model. Am J Physiol Heart Circ Physiol. 2004; 287:1663–1669.
36. Kroon, D.; Slump, CH. Coherence filtering to enhance the mandibular canal in cone-beam CT data; Annual symposium of the IEEE-EMBS benelux, Chapter 2009; Enschede, the Netherlands. 2009.
37. Hollander Y, Durban D, Lu X, Kassab GS, Lanir Y. Constitutive modeling of coronary arterial media-comparison of three model classes. J Biomech Eng. 2011; 133:061008. [PubMed: 21744928]
38. Dobrin PB. Influence of initial length on length-tension relationship of vascular smooth muscle. Am J Physiol. 1973; 225:664–670. [PubMed: 4726501]
39. Chen H, Liu Y, Slipchenko MN, Zhao XF, Cheng JX, Kassab GS. The layered structure of coronary adventitia under mechanical load. Biophys J. 2011; 101:2555–2562. [PubMed: 22261042]
40. Chen H, Zhao X, Lu X, Kassab G. Non-linear micromechanics of soft tissues. Internat J Non-Linear Mech. 2013 in press.
41. Sacks MS. Incorporation of experimentally-derived fiber orientation into a structural constitutive model for planar collagenous tissues. J Biomech Eng. 2003; 125:280–287. [PubMed: 12751291]
42. Stella JA, Liao J, Hong Y, David Merryman W, Wagner WR, Sacks MS. Tissue-tocellular level deformation coupling in cell micro-integrated elastomeric scaffolds. Biomaterials. 2008; 29:3228–3236. [PubMed: 18472154]
43. Ingber DE. Cellular mechanotransduction: putting all the pieces together again. FASEB J. 2006; 20:811–827. [PubMed: 16675838]
44. Timmins LH, Wu Q, Yeh AT, Moore JE, Greenwald SE. Structural inhomogeneity and fiber orientation in the inner arterial media. Am J Physiol Heart Circ Physiol. 2010; 298:1537–1545.
45. Verlohren S, Dubrovska G, Tsang SY, Essin K, Luft FC, Huang Y, et al. Visceral periadventitial adipose tissue regulates arterial tone of mesenteric arteries. Hypertension. 2004; 44:271–276. [PubMed: 15302842]

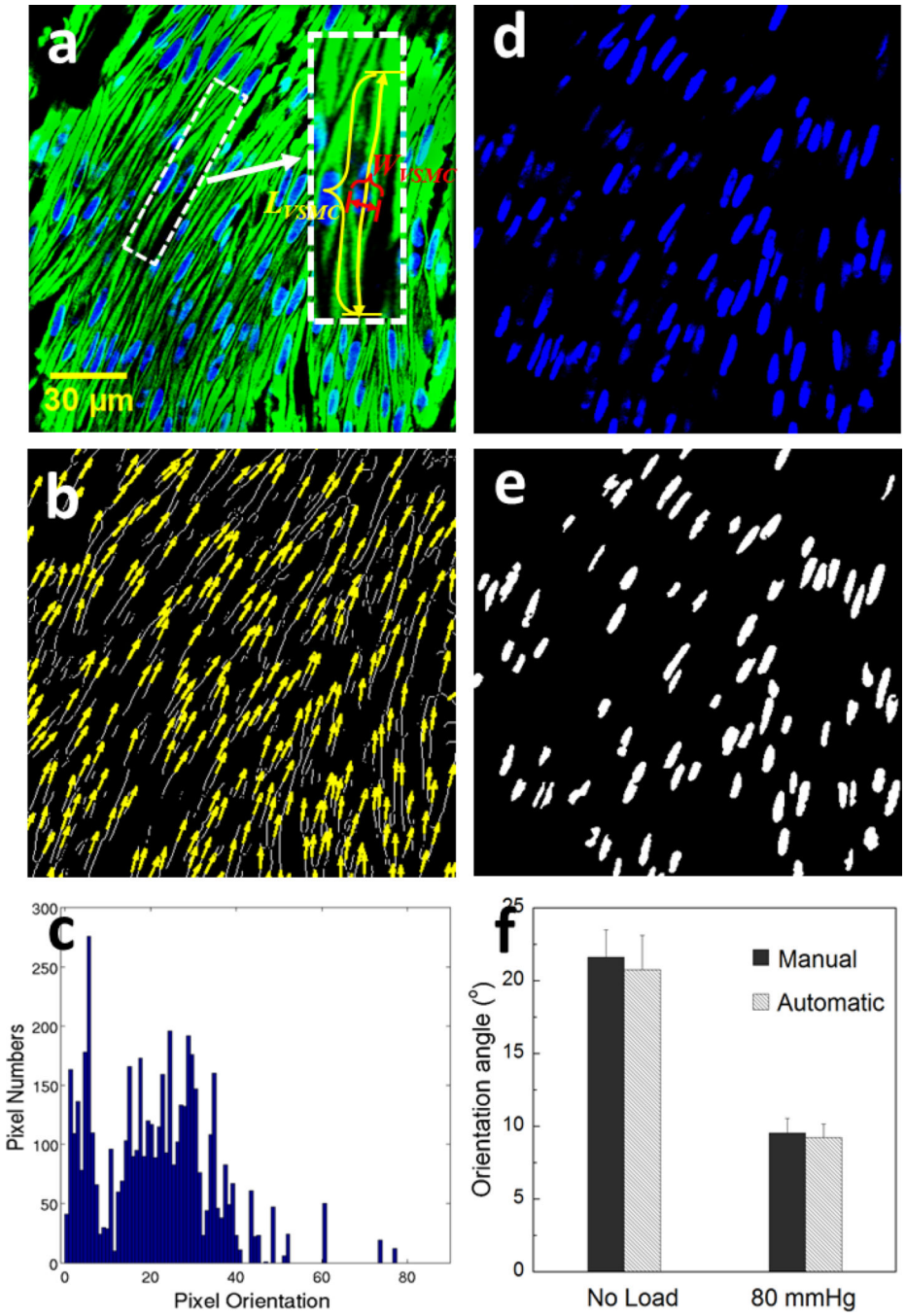

Figure 1.

Experimental measurements of VSMC geometries. (a) Dimensions of a single VSMC, L_{VSMC} is the length and W_{VSMC} is the width; (b) Automatical measurement of VSMC orientations based on cell center-lines; (c) The histogram frequency distribution of VSMC orientations of a selected image. (d) The RGB image (Blue) of the cell nucleus; (e) Image processed by median filtering; (f) Comparison between manually and automatic measurements of VSMC orientation angle.

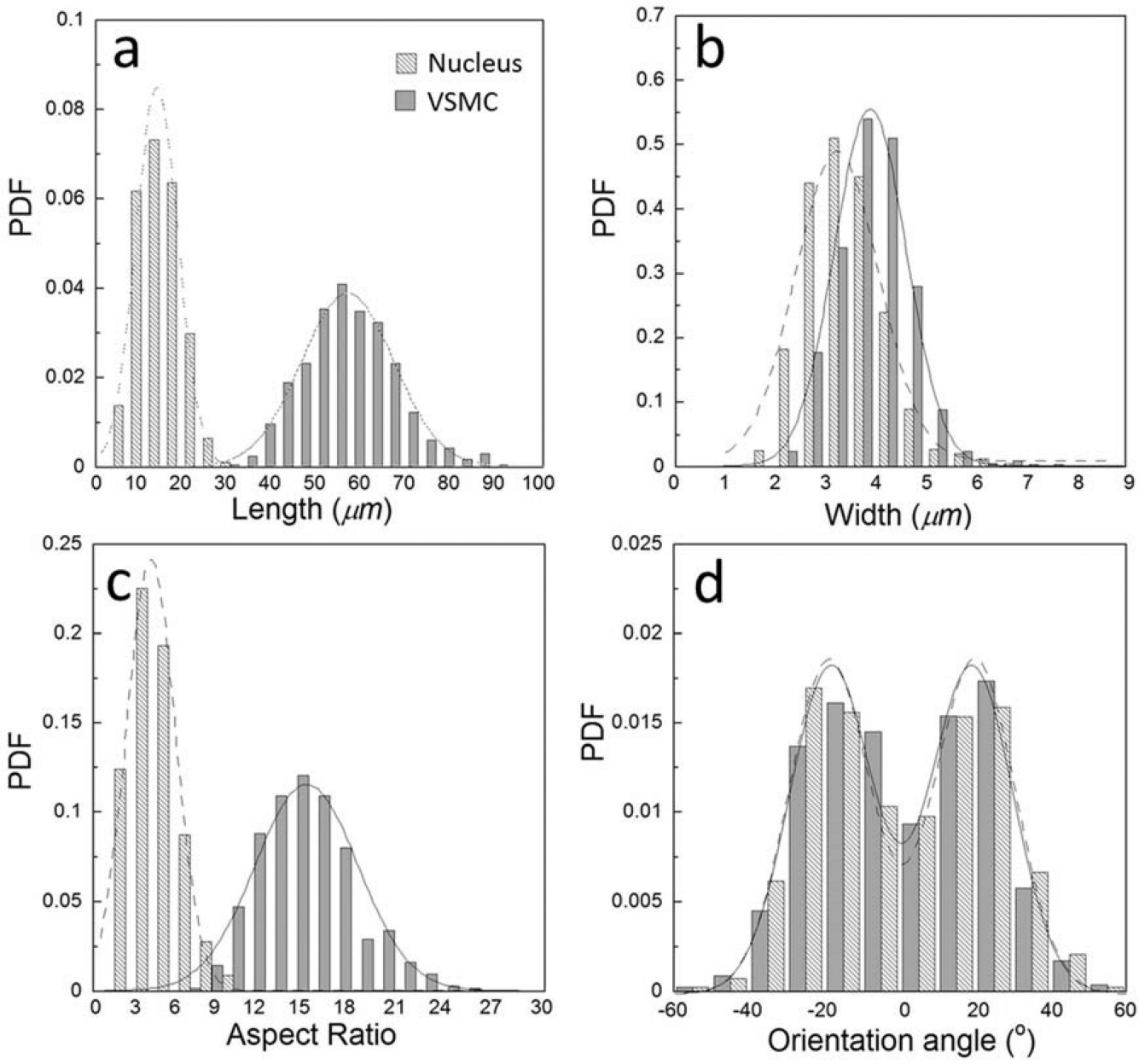

Figure 2.

Distribution of VSMC geometrical parameters at ZSS. (a) Probability density functions (PDFs) of the lengths of VSMC and the nucleus; (b) PDFs of the widths of VSMC and the nucleus; (c) PDFs of the aspect ratios of VSMC and the nucleus; (d) PDFs of the orientation angles of VSMC and the nucleus. Columns present experimental measurements, and solid and dashed lines present normal distributions of geometrical parameters of VSMC and the nucleus, respectively.

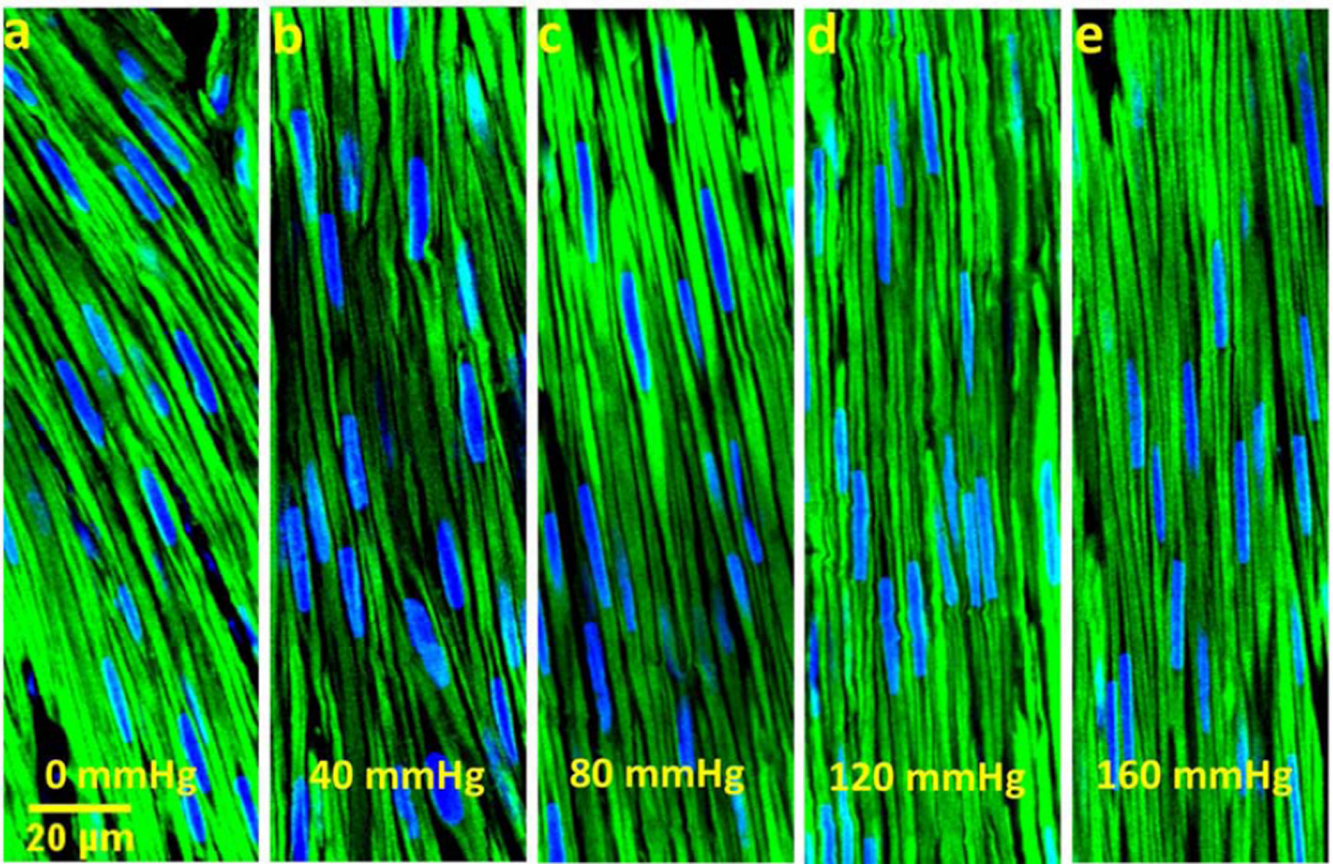

Figure 3.

The deformed VSMCs of coronary media under various distention pressures: The loading pressures in (a)-(e) are: 0 mmHg, 40 mmHg, 80 mmHg, 120 mmHg, 160 mmHg, respectively.

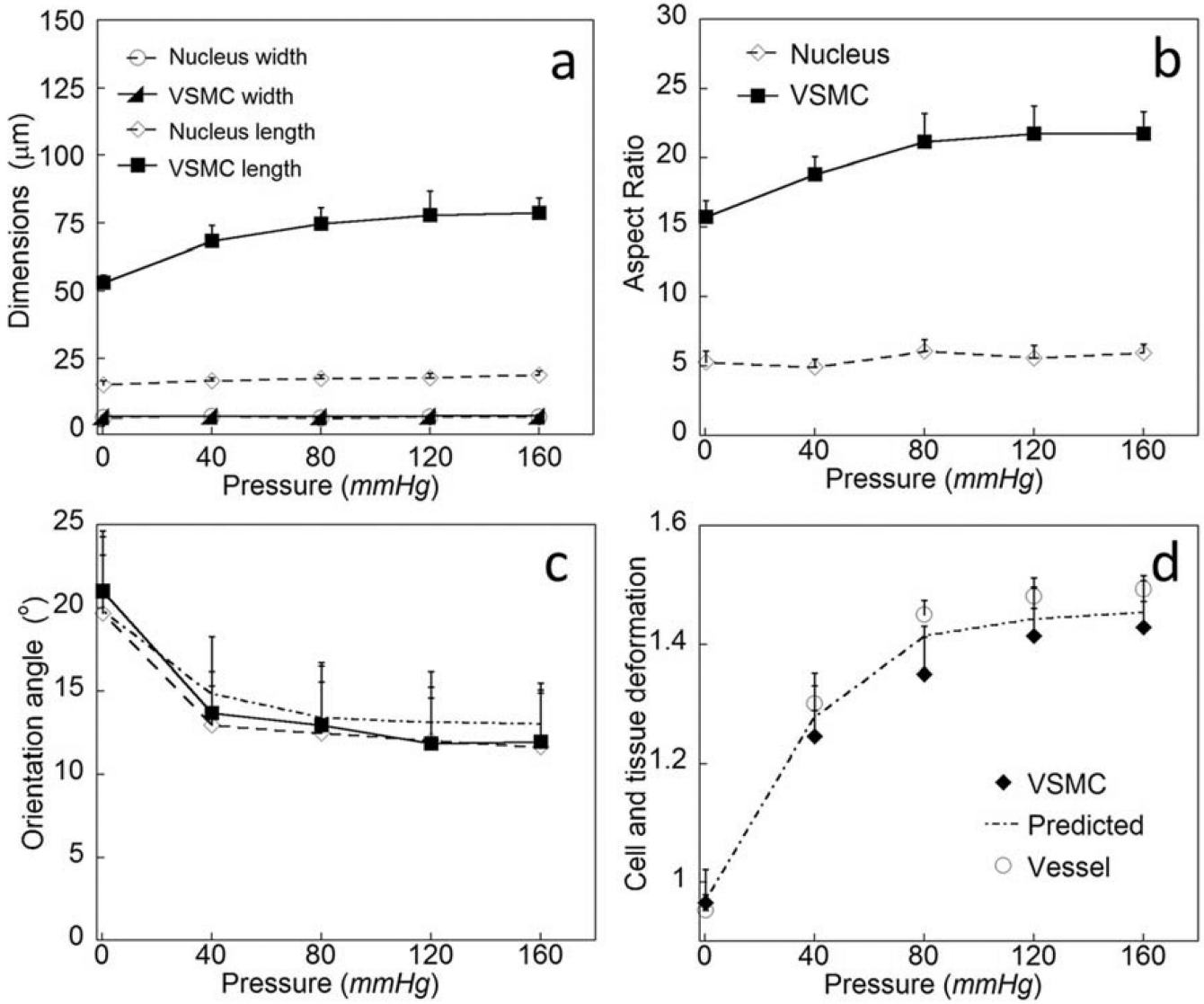

Figure 4.

The nonlinear parameter-pressure relations of VSMC and the nucleus of coronary media. With the increase of distension pressure, (a) Changes of the length and with; (b) Change of the aspect ratio; (c) Measured and predicted changes of the orientation angle; (d) Measured and predicted VSMC and tissue deformation.

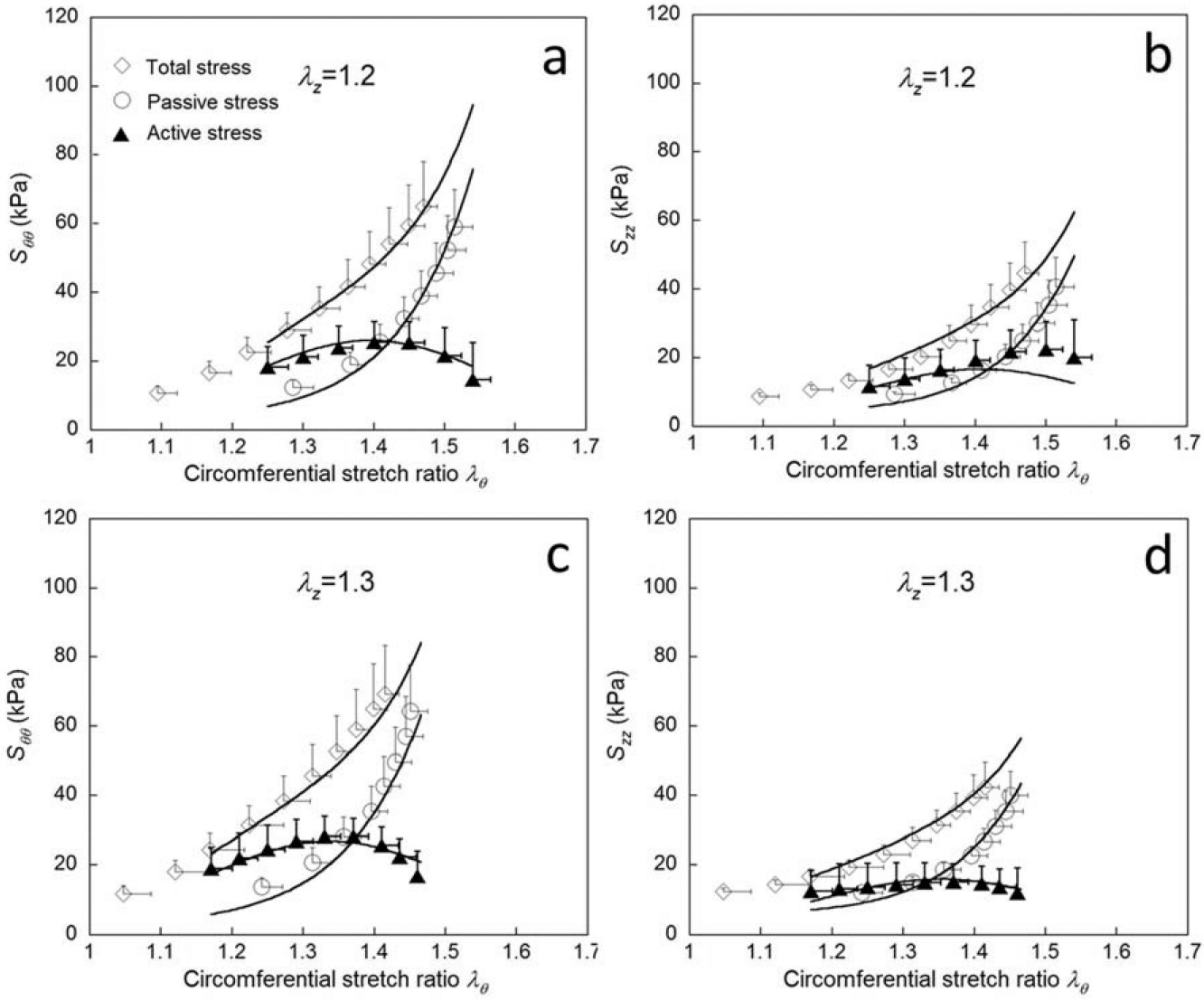

Figure 5.

The second Piola-Kirchhoff total, passive and active stresses of coronary media. (a) The circumferential stresses at $\lambda_z = 1.2$; (b) The axial stresses at $\lambda_z = 1.2$; (c) The circumferential stresses at $\lambda_z = 1.3$; (d) The axial stresses at $\lambda_z = 1.3$. Symbols present experimental measurements, and solid lines present the predicted values from theory.

Biomaterials. Author manuscript; available in PMC 2014 October 01.

Table 1

The distribution of geometrical parameters of VSMC and the nucleus were fitted to a continuous normal distribution (or a bimodal normal distribution) $f(x)=\frac{1}{\sigma\sqrt{2\pi}}e^{\frac{(x-\mu)^2}{2\sigma^2}}$, where μ is the mean of the distribution and σ is standard deviation.

	Nucleus			VSMC		
Parameters	**μ**	**σ**	R^2	**μ**	**σ**	R^2
Length (μ*m*)	15.0	4.7	0.96	56.0	10.3	0.98
Width (μ*m*)	3.4	0.8	0.85	3.9	0.7	0.93
Aspect ratio	4.6	1.7	0.80	14.7	3.5	0.88
Orientation (°)	±19.9	10.7	0.98	±18.7	10.9	0.92

Table 2

Non-linear relations between geometrical parameters and distension pressures obtained by curve fitting to a logarithmic function: $y = a_1 + a_2 Log(x)$

	Parameters	a_1	a_2	R^2
VSMC	Length (μm)	60.2	7.7	0.95
	Aspect Ratio	17.4	1.8	0.90
	Orientation (°)	18.2	−2.9	0.99
	Stretch Ratio	1.1	0.1	0.95
Nucleus	Length (μm)	16.1	0.9	0.81
	Orientation (°)	17.2	−2.5	0.99

Table 3

Material parameters of the microstructural model (Eq. 3) of passive coronary media

Animal No.	k_E **(kPa)**	k_C **(MPa)**	N_C	θ_C **(°)**	R^2 **for** $S_{\theta\theta\ passive}$	R^2 **for** $S_{zz\ passive}$
Sample 1	43.2	6.4	5.6	36.4	0.99	0.97
Sample 2	40.1	2.2	5.3	50.5	0.99	0.91
Sample 3	68.7	1.2	4.2	38.4	0.99	0.93
Sample 4	64.7	4.2	5.5	31.2	1.00	0.98
Sample 5	53.3	1.8	4.0	38.5	0.99	0.99
Mean±SD	54.0±11.3	3.1±1.9	4.9±0.7	9.0±6.3		
Fit of all data of Sample 1–5	40.5	5.4	5.6	0.7	1.00	1.00

Table 4

Material parameters of two-dimensional strain energy function (Eq. 6) of active VSMC of coronary media

Animal No.	C_{act} (kPa)	b_1	b_2	b_3	b_4	$\lambda'_{SMC-1.2}$*	$\lambda'_{SMC-1.3}$*	b_1/b_2	R^2 for $S_{\theta\theta active}$	R^2 for $S_{zz\ active}$
Sample 1	9.7	0.2	0.5	1.4	1.3	1.41	1.36	0.4	0.80	0.83
Sample 2	5.1	0.3	0.8	1.4	1.4	1.44	1.41	0.3	0.87	0.78
Sample 3	4.2	0.2	0.4	1.4	1.2	1.39	1.35	0.4	0.89	0.93
Sample 4	15.7	0.2	0.4	1.4	1.5	1.53	1.47	0.5	0.97	0.73
Sample 5	16.8	0.3	0.6	1.3	1.3	1.37	1.32	0.5	0.81	0.82
Mean±SD	10.3±5.2	0.2±0.04	0.5±0.2	1.4±0.02	1.3±0.1	1.43±0.06	1.38±0.05	0.4±0.06		
Fit of mean of Sample 1–5	8.1	0.2	0.5	1.3	1.4	1.41	1.36	0.5	0.91	0.62

*$\lambda'_{SMC-1.2} = b_3 - b_1(1.2 - b_4)/b_2$ is VSMC optimal stretch ratio at axial stretch ratio λ_z = 1.2, and $\lambda'_{SMC-1.3} = b_3 - b_1(1.3 - b_4)/b_2$ is VSMC optimal stretch ratio at λ_z = 1.3.